Mechanical Behavior of Particulate Composites: Experiments and Micromechanical Predictions

F. C. WONG[1,2] and A. AIT-KADI[1,*]

[1]CERSIM, Department of Chemical Engineering, Laval University, Quebec, Quebec, G1K 7P4, Canada, and [2]Defence Research Establishment Valcartier, Courcelette, Quebec, G0A 1R0, Canada

SYNOPSIS

A model, based on linear elasticity and the first law of thermodynamics, was evaluated using experimentally derived data to verify its predictive capabilities. The model demonstrated that it could correctly predict the mechanical behavior of highly loaded composites if a representative adhesion energy was available. It worked well for systems where material nonlinearity was mainly due to particle debonding. The model could not, however, account for the effects of localized straining or stress concentrations on composite modulus or strength. In systems where matrix nonlinearity dominated, predictions were less satisfactory. Although the model oversimplified the debonding process, it provided a convenient mechanism for relating the composite modulus and stress–strain state to the loss of reinforcement without requiring a micromechanical description that was too cumbersome to manage. Nevertheless, the inability of the model to account for localized strains, stress concentrations, and matrix nonlinearity needs to be addressed in order to obtain better mechanical behavior predictions. © 1995 John Wiley & Sons, Inc.

INTRODUCTION

Use of fillers in conjunction with polymers to improve mechanical, physical, optical, and electrical properties has been commonplace since the beginning of the plastics industry.[1,2] Particulate composite materials have been employed typically for high-volume products such as rubber tires, automotive panels, appliance housings, and conduits. In the aerospace industry, particulate composites have come in the form of highly filled propellants used in solid rocket motors. Not only is there a scientific interest in the analysis of such systems but there is also a practical interest. The prediction of mechanical properties based on the knowledge of filler and matrix properties gives designers greater latitude in material selection.

Many experimental investigations have been carried out to identify the parameters that govern mechanical behavior. Generally, it has been found that:

1. Reinforcement increases with decreasing particle size.[3–6]
2. Reinforcement increases with increasing adhesion.[7–10]
3. Increase filler concentration increases composite modulus.[11–13]

Particulate composite analysis techniques have ranged from semiempirical to micromechanical analyses. Semiempirical approaches isolate important parameters by making them variables.[14–16] Micromechanical analyses come in the form of variational formulations or approximations. Variational approaches have been used to relax the requirements that interface boundary conditions around each particle be satisfied exactly.[17–20] Approximations have been used with the hope that the errors introduced by the approximations are not large.[21] This technique has been used widely because of the variety of approximations possible.[22–25] Researchers have always had to struggle with the level of detail to include in their models. Too little detail would result in inaccurate predictions; too much detail would result in intractable problems.

Most of the theories used to study particulate

* To whom correspondence should be addressed.

Journal of Applied Polymer Science, Vol. 55, 263–278 (1995)
 CCC 0021-8995/95/020263-16

composites have been concerned primarily with the prediction of the modulus. Of greater interest is a technique that would permit prediction of overall stress–strain behavior. Anderson and Farris[26,27] developed such a model based on classical linear elastic analysis and the first law of thermodynamics. The model appears to contain many of the parameters necessary to account for experimentally observed composite behavior as well as being formulated in a tractable manner. The purpose of this work is to evaluate the strengths and weaknesses of the Anderson–Farris model using experimentally derived data and to show that it can serve as a useful foundation for further work.

THEORY

The Anderson–Farris model[26,27] is based on the principle that the work energy put into the material must be either stored as internal strain energy or be used to create new surface area through the process of debonding between particle and matrix or be some combination of the two. The assumptions made in the formulation of the model were:

1. The particulate and matrix materials are linear elastic.
2. The nonlinear stress–strain behavior is due to the debonding process only.
3. The overall material can be considered homogeneous.

Assumption 2 excludes any energy that may be dissipated through viscoelastic losses in the matrix or any energy that may be dissipated through friction between the matrix and filler. Assumption 3 implies that the representative volume element is larger than the largest particle. Thus, average stress, average strain, and average modulus can be calculated. Its validity depends upon the insignificance of stress concentrations created by the presence of the filler.

Changes in internal stress state were related to the debonding process through a modified first law of thermodynamics,

$$\delta Q + \delta W = \delta U + G_c \delta A \tag{1}$$

where δQ is the net heat transferred into system, δW the net external work done on system, δU the net internal energy in system, and $G_c \delta A$ the surface energy dissipated.

Considering that the work input was carried out under adiabatic conditions and using the usual virtual work equations for structural mechanics,[28] the energy released was shown to be related to the variations in the material stress and strain by

$$2G_c \frac{\delta A}{V_0} = \sigma_{ij} \delta \epsilon_{ij} + \delta \sigma_{ij} \epsilon_{ij} \tag{2}$$

This equation combined the effects of internal strain energy and work into one term and so departed from the usual technique used when analyzing structures using virtual work principles.

Anderson[27] used Eq. (2) along with the constitutive equation for isotropic linear elastic solids to derive an equation applicable for a uniaxial tensile test under a superimposed pressure. In Ref. 26, two models were proposed. One was called the concentration decrease (CD) model and the other was called the void addition (VA) model. The CD model approximated the changes in modulus by eliminating the debonded particle from the composite and replacing it with matrix. When all particles had debonded, the composite was comprised of matrix only. The VA model approximated modulus changes by keeping the debonded particle and adding a void of equivalent size to the matrix. Thus, the composite occupied more volume at the end of particle debonding than at the beginning. Later, a third model called, appropriately, the combined model was a combination of the CD and VA models.[27] This model was found to give the best results. The combined model eliminated the debonded particle from the composite and replaced it with a void of equivalent size. All particles were eventually replaced by voids.

The final equation for a uniaxial tensile bar under atmospheric pressure was

$$-2 \frac{G_c}{V_0} \left(\frac{dA}{dc} \right) = \epsilon_{11}^2 \left(\frac{dE}{dc} \right) \tag{3}$$

where G_c is the adhesion energy, V_0 the unit volume, A the debonded surface area, c the current filler concentration, ϵ_{11} the uniaxial strain, and E the composite modulus.

The change in surface area in relation to the change in concentration in terms of particle radius, r, was

$$\frac{dA}{dc} = -6V_0/r \tag{4}$$

This equation took into account the fact that two surfaces were created when a particle was debonded, one in the matrix and one on the filler. Modulus

changes based on concentration were calculated using the Farber–Farris equations:[29]

$$\frac{dG}{dc} = \frac{-15G(1-\nu)\left(1-\frac{G_i}{G}\right)}{\left(7-5\nu+2(4-5\nu)\frac{G_i}{G}\right)\left(1-\frac{c}{P_f}\right)} \quad (5)$$

$$\frac{dK}{dc} = \frac{K_i - K}{\left(1+\frac{K_i-K}{K+\frac{4}{3}G}\right)\left(1-\frac{c}{P_f}\right)} \quad (6)$$

where G is the shear modulus of composite, ν Poisson's ratio of composite, K the bulk modulus of composite, K_i, G_i the moduli of filler, c the current filler volume fraction, and P_f the maximum packing fraction.

The equations were derived using an effective medium technique that assumed filler was being added or subtracted from a composite that had homogeneous properties. Numerical integration of Eqs. (5) and (6) was started by setting the composite shear modulus, G, and the composite Poisson's ratio, ν, equal to the matrix shear modulus, G_m, and the matrix Poisson's ratio, ν_m. The composite Poisson ratio and modulus, E, were recovered from Eqs. (5) and (6) through the classical linear elastic relationships:

$$\nu = \frac{3K - 2G}{2(3K + G)} \quad (7)$$

$$E = 2G(1 + \nu) \quad (8)$$

Using Eqs. (3)–(8), the critical strain to debond a particle of a particular diameter could be calculated knowing the state of adhesion and the mechanical properties of the constituent materials.

The implementation of Eqs. (3)–(8) in a computer program to predict stress–strain behavior mimicked the physical processes thought to occur in the composite as it deformed. The algorithm can be summarized as follows:

Constituent properties and initial composite configuration:

1. Specify mechanical properties of the matrix and filler and adhesion energy.
2. Specify initial concentration of voids and statistical distribution of filler.

Deformation of composite:

3. Determine largest particle size for current iteration.
4. Calculate composite properties E, K, dE/dc, and dK/dc.
5. Calculate critical strain for particle diameter.
6. Calculate critical stress using current composite properties.
7. Reduce filler concentration and increase void concentration by equivalent amount.
8. Repeat calculation starting from step 3 until there are no particles remaining.

EXPERIMENTAL

Materials

High-density polyethylene (HDPE) and spherical glass beads were chosen as constituent materials for the model composite material because their processing properties and mechanical behavior are well known. The HDPE used (DOW Chemical Series 32060C) was an extrusion-grade resin that has a Melt Flow Index (MFI) of 0.32 g/10 min and a nominal density of 0.960 g/cm^3. Large and small diameter glass beads were obtained from Potters Industries. Stock size 2227 had an advertised average diameter of 100 μm while Stock size 2900 had an average diameter of 25 μm. Surface modification of the glass beads was carried out using the UCARSIL PC series of organofunctional silanes produced by Union Carbide.

There were two objectives for the experimental portion of this work. The first objective was to characterize as accurately as possible the parameters required in the theoretical model. The second objective was to fabricate an assortment of model composites in order to obtain a range of mechanical behavior. The test matrix shown in Table I evaluates the effects of surface treatment, filler volume fraction, and particle size on mechanical behavior. Each composite designation is composed of a letter (U or T) indicating the surface treatment followed by a number (100 or 25 μm) identifying the particle size and then ending with another number (50 or 20%) showing the nominal filler volume fraction.

Table I Test Matrix of Composites Used to Show Effects of Particle Size, Filler Volume Fraction, and Surface Treatment

		Untreated	Treated
50% loading	100 μm	U100-50	T100-50
	25 μm	U25-50	T25-50
20% loading	100 μm	U100-20	T100-20
	25 μm	U25-20	T25-20

Table II Material Feed Rates, Barrel Temperatures, and Rotor Speeds Used During Fabrication of Composites[a]

Composite	HDPE Feed Rate (g/min)	Glass Feed Rate (g/min)	Silane Feed Rate (g/min)	Rotor Speed (rpm)
HDPE	30.0	—	—	60
U100-50	10.0	26.0	—	30
T100-50	9.8	25.6	0.520	30
U100-20	29.7	18.0	—	38
T100-20	29.2	19.6	0.365	40
U25-50	9.5	24.0	—	30
T25-50	9.6	26.8	0.486	30
U25-20	29.0	19.9	—	40
T25-20	29.1	19.8	0.378	40

[a] Barrel temperatures: zone 1 (feed), 155°C; zone 2, 165°C; zone 3, 180°C, die, 190°C.

The tensile test specimens were fabricated in a two-step process. The base mix was prepared using a Haake-Buchler Rheocord System 40 with a conical twin-screw extruder. An exit die with four 3.2-mm nozzles was used. HDPE and glass beads were fed simultaneously into the extruder using custom-built screw feeders. To prevent overloading the extruder drive train with the introduction of filler into the polymer, the filler mass flow rate was gradually increased until the desired rate was reached. The extruded composite was quenched in water upon exit from the die. The silane coupling agent (3 : 1 ratio by weight of UCARSIL PC-2B to UCARSIL PC-1B) was added to the HDPE and glass beads in the extruder at a rate of 2% by weight of the glass feed rate.[30] Precise metering of the agent was achieved using a Buchler Polystaltic Pump Model 2-6150 and Cole Palmer 0.76-mm ID tubing. Table II shows the HDPE, glass bead, and silane coupling agent feed rates as well as the barrel temperatures used for each of the composites in the test matrix. The HDPE and glass beads were dried under vacuum at 60°C for at least 12 h before use to remove trace moisture.

Test specimen dimensions are shown in Figure 1. The specimen, known as a JANNAF Class C specimen, was developed by the JANNAF committee and is suited particularly for highly loaded materials.[31] Fabrication of the specimens was accomplished using a transfer molding technique. The base material was pelletized, preheated, and then delivered using a 150-ton press into a preheated eight-specimen mold. The specimens were demolded and allowed to air cool afterward.

Procedure

Prior to base material fabrication, each batch of glass beads was sized using a Malvern Series 2600C particle sizer and a PS64 dry powder feeder. The instrument was set up to measure particles sizes in the range of 1.9 to 188 μm. A lognormal model was used to reduce the data to obtain mean and standard

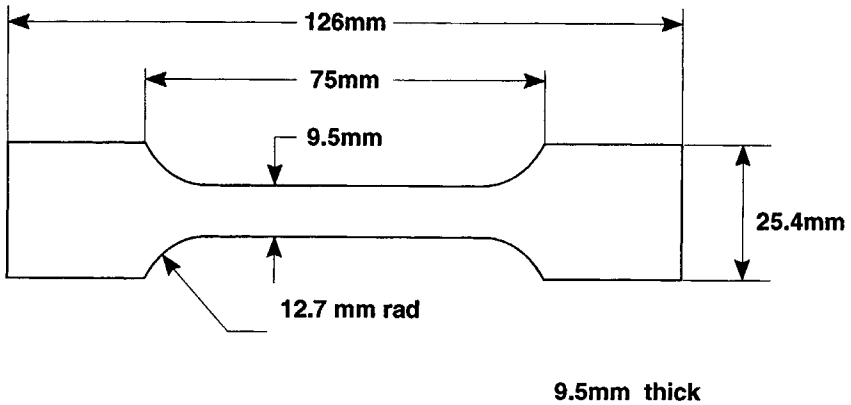

Figure 1 Dimensions for JANNAF Class C tensile test specimen.

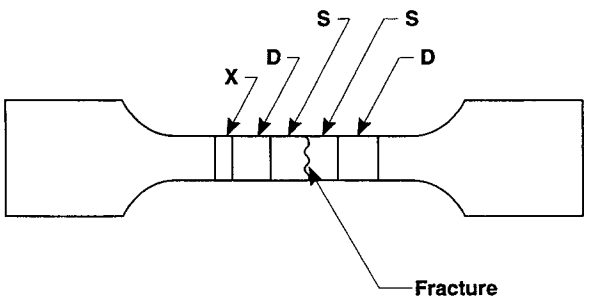

Figure 2 Dissection scheme to obtain density, crystallinity, and fracture surface samples.

deviation values. Three to five trials were performed for each stock size.

The JANNAF specimens were tested at 20°C in an Instron 4206 at 10 mm/min crosshead speed. Specimens were preconditioned in a vacuum desiccator for 24 h at room temperature. Six specimens were tested for each composite combination. Statistical results for initial modulus, secant modulus, maximum stress, and strain at maximum stress were obtained using Instron Series IX software.

The filler volume fraction was calculated using a rearranged form of the rule of mixtures equation for composite density. Density measurements were carried out by immersing dissected blocks from the tested specimens in hexane according to ASTM D792-91.[32] A diagram of the dissection scheme is shown in Figure 2. Two specimens were weighed and the results were averaged.

The crystallinity of the HDPE directly affects the mechanical properties of the polymer.[33] Crystallinity for each composite was measured by differential scanning calorimetry (DSC) using a DuPont DSC 910 to confirm that it, and therefore the polymer modulus, had not changed significantly from one composite to the next. Blocks of composite were cut from the location shown in Figure 2. Crystallinity was calculated according to the standard method[34] using a melting enthalpy that was corrected for the reduced quantity of HDPE found in each composite.

Error on the filler volume fraction, density, and crystallinity measurements were estimated by differentiating the equations used to calculate the results. The error, therefore, only accounts for the variations in the dependant variables used to calculate the result.

RESULTS AND DISCUSSION

Particle Size, Density, Volume Fraction, and Crystallinity

Tables III and IV show the particle size results from the Malvern. Examination of the histograms produced by the Malvern software showed that the majority of the particles for Stock 2227 fell in the 113–160-μm range (Table III) while Stock 2900 had a much broader distribution (Table IV). The standard deviation, N, was given by the Malvern Mastersizer software. The implementation of the Anderson–Farris model used log standard deviation. This value is shown as n in the tables.

Samples for the filler volume fraction, density, and crystallinity measurements were dissected from test specimens that exhibited average mechanical behavior. Density, filler volume fraction, and crystallinity results are shown in Table V. The density of the pure HDPE specimen fell within accepted limits.[35] Filler volume fraction calculations assumed there were no voids or density changes between the pure HDPE specimens and the HDPE contained in the composites. Given the error in the volume fraction values (Table V), this could easily encompass the actual void content, thus making an exact determination of void content difficult. The measurements demonstrated that calibration of the screw feeders was fairly accurate in all cases except for U100-50, which was on the low side.

The crystallinity values show that, in general, the crystallinity was in the 60% range for all composites. It is interesting to note that the crystallinity was slightly higher in the lowly loaded materials. This

Table III Particle Size Distribution of Potters Industries Stock 2900 as Measured Using Malvern Particle Sizer[a]

Size (μm)	% Under	Size Band (μm)	%
188.0	100		
87.2	99.7	188.0–87.2	0.3
53.5	92.4	87.2–53.5	7.3
37.6	69.6	53.5–37.6	22.8
28.1	40.1	37.6–28.1	29.5
21.5	17.2	28.1–21.5	22.9
16.7	5.4	21.5–16.7	11.8
13.0	1.2	16.7–13.0	4.2
10.1	0.2	13.0–10.1	1.0
7.9	0.0	10.1–7.9	0.2

[a] Average diameter (d_{avg}), 31 μm; standard deviation (N), 1.47; log std. deviation (n), 0.167.

Table IV Particle Size Distribution of Potters Industries Stock 2227 as Measured Using Malvern Particle Sizer[a]

Size (μm)	% Under	Size Band (μm)	%
564.0	100		
261.7	100	564.0–261.7	0.6
160.4	99.4	261.7–160.4	91.5
112.8	7.9	160.4–112.8	7.9
84.3	0.0	112.8–84.3	0.0

[a] Average diameter (d_{avg}), 130 μm; standard deviation (N), 1.09; log std. deviation (n), 0.0374.

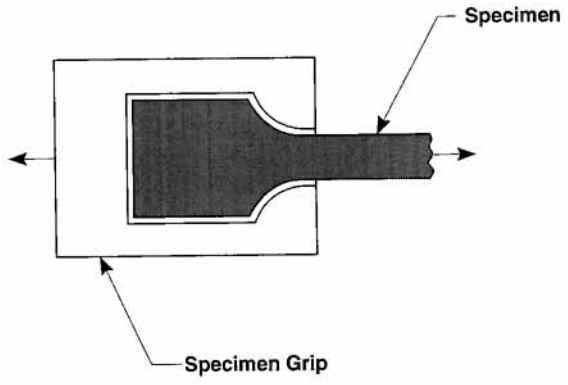

Figure 3 JANNAF Class C specimen grip and specimen installation.

increase could be due to the slower cooling rates experienced by the increased mass of polymer. Furthermore, for composites T25-50 and T100-20, comparison of density and crystallinity values indicate that higher densities and crystallinity could be due to the increased surface contact between bead and polymer, which is promoted by the silane treatment. Since the crystallinity calculations were based on filler volume fractions, which themselves were based on the assumption of no voids, the proximity of all crystallinity values to 60% indicated that the modulus measured with the pure HDPE specimens could be considered a representative value for the HDPE modulus in the other composites.

Mechanical Properties

The JANNAF specimen was tested using grips that applied the displacement through the shoulders of the specimen (Fig. 3). End tabs could have been used, but finding an adhesive that could withstand the high loads without debonding was a problem. Pneumatic grips were another option, but they had the problem of producing grip failures if the clamping pressure was too high or slippage if the clamping pressure was too low.

It is well known in the solid propellant community that for this type of test configuration, the displacement applied to the grips is not necessarily the displacement transmitted into the test section. The reason for this is that the material in the shoulder area deforms. To compensate for this deformation, an effective gauge length must be used with the crosshead displacement to determine strain.[36]

Effective gauge length (EGL) is determined by trial and error through comparison of the actual strain with the strain calculated from crosshead displacement. Actual strain in the specimen test section was measured during a tensile test with an OPTRA Laser Extensometer (OPTRA Inc., Peabody, MA). Figure 4 shows the absolute error and the ratio of the crosshead strain (e_{Xhead}) to the actual strain (e_{ac}) versus the actual strain for T25-20. In general, the strain is overestimated by the crosshead strain at the beginning of the test; later, it is underestimated. The ratio of the two strain measures (e_{Xhead}/e_{ac}) shows initial moduli determined using actual strains will be two to three times higher than initial moduli determined using crosshead strains. The ratio drops quickly afterward to a value of 1. At that point, the

Table V Density, Filler Volume Fraction, and Crystallinity Results for HDPE–Glass Bead Composites

Composite	Density (g/cm^3)	Volume Fraction	Crystallinity (%)
HDPE	0.949 ± 0.002	—	65
U100-50	1.591 ± 0.003	0.43 ± 0.02	56 ± 2
T100-50	1.686 ± 0.003	0.49 ± 0.03	59 ± 4
U100-20	1.206 ± 0.002	0.17 ± 0.01	57 ± 1
T100-20	1.231 ± 0.002	0.19 ± 0.01	64 ± 1
U25-50	1.666 ± 0.003	0.48 ± 0.02	58 ± 2
T25-50	1.691 ± 0.003	0.49 ± 0.03	58 ± 4
U25-20	1.234 ± 0.002	0.19 ± 0.01	64 ± 1
T25-20	1.272 ± 0.002	0.22 ± 0.01	62 ± 1

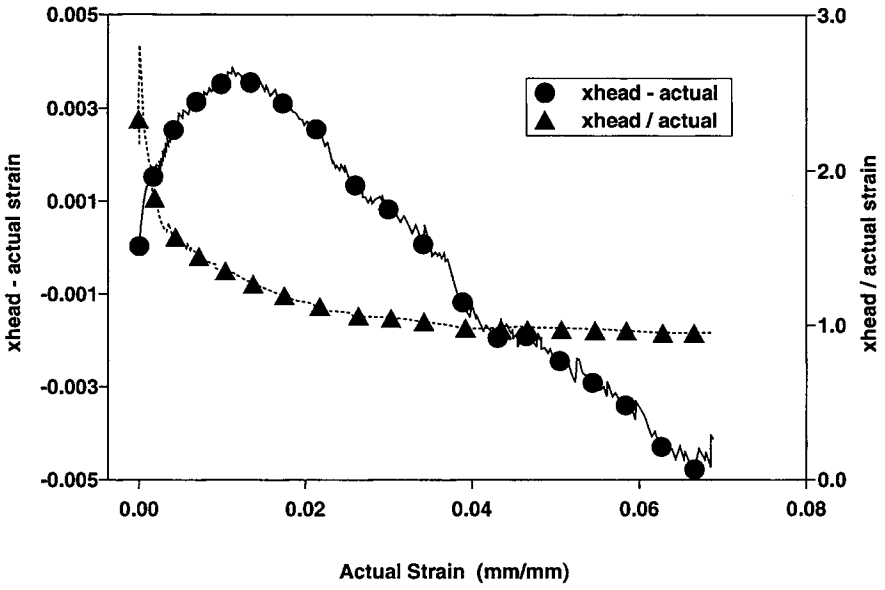

Figure 4 Relationship between crosshead strain and actual strain for T25-20.

crosshead strain and actual strain are virtually identical. Effective gauge length values along with the associated mechanical properties are given in Table VI. Only one specimen from each composite was used to generate the table. Comparison of EGL with the corresponding modulus shows that, in general, EGL is proportional to modulus.

The laser extensometer was not used for all mechanical property testing because it had a tendency to lose its signal momentarily during a test. This would cause the extensometer to zero itself before continuing on with strain measurement. Since the Instron Series IX software was being used for data acquisition and reduction, the occasional resetting of the strain interfered with the statistical calculations for strain at maximum stress and modulus. The Series IX software allowed the user to enter in a gauge length so it was safer to base strain measurement on the crosshead displacement rather than the laser extensometer.

Table VII summarizes the mechanical property data collected for all composites. The error given in the table represents data scatter. Figures 5–7 illustrate the same results but group them according to property and treatment.

The data showed that all composites with 50%

Table VI Summary of Mechanical Properties Obtained from Uniaxial Tensile Tests Done at 10 mm/min, 20°C[a]

Composite	E_{ac} (MPa)[b]	σ_{max} (MPa)[c]	e_{max} (%)[d]	EGL (mm)[e]
HDPE	2012	28.1	10.4	77.0
U100-50	2430	10.7	6.4	78.5
T100-50	6170	20.1	1.0	145.0
U100-20	1880	20.4	8.4	84.5
T100-20	2910	39.0	7.7	93.5
U25-50	2290	10.5	0.9	83.0
T25-50	11600	28.4	1.7	140.0
U25-20	2180	18.7	9.7	72.3
T25-20	3950	39.6	6.6	97.0

[a] Strain measurement based on laser extensometer.
[b] E_{ac}, actual initial modulus.
[c] σ_{max}, maximum stress.
[d] e_{max}, strain at maximum stress.
[e] EGL, effective gauge length.

Table VII Summary of Mechanical Properties Obtained from Uniaxial Tensile Tests Done at 10 mm/min, 20°C[a]

Composite	E_s (MPa)[b]	σ_{max} (MPa)[c]	e_{max} (%)[d]	E_i (MPa)[e]	E_i/E_s
HDPE	500 ± 10	27.8 ± 0.7	10.2 ± 0.5	860 ± 10	1.72
U100-50	520 ± 110	9.3 ± 0.4	4.4 ± 0.7	1140 ± 120	2.19
T100-50	3670 ± 50	21.1 ± 0.1	0.73 ± 0.03	4440 ± 100	1.21
U100-20	500 ± 10	20.6 ± 0.9	8.2 ± 0.4	1210 ± 100	2.42
T100-20	1110 ± 30	29.6 ± 1.5	5.9 ± 0.9	1640 ± 20	1.48
U25-50	1770 ± 70	12.2 ± 0.6	0.77 ± 0.04	1930 ± 100	1.09
T25-50	3700 ± 90	29.2 ± 0.3	1.3 ± 0.1	4610 ± 50	1.25
U25-20	456 ± 20	19.8 ± 0.8	9.1 ± 0.7	1180 ± 50	2.59
T25-20	990 ± 10	34.3 ± 1.7	6.0 ± 0.2	1730 ± 60	1.75

[a] Strain measurement based on crosshead displacement.
[b] E_s, secant modulus.
[c] σ_{max}, maximum stress.
[d] e_{max}, strain at maximum stress.
[e] E_i, initial modulus.

filler concentration had lower load-carrying capability than their 20% counterparts (Fig. 5). In general, the composites containing 25-μm beads had higher strength than the composites containing 100-μm beads. This agreed with other studies.[3-6] The exception was between U100-20 and U25-20, which had the same strength. In all cases, the composites with treated beads had higher maximum stresses than their corresponding composites with no treatment. This showed that the method used to add the silane to the composite was adequate and that the adhesion between bead and HDPE had improved.

The strain at maximum stress for highly loaded composites was always lower than that for lowly loaded composites (Fig. 6). This behavior has been seen before.[37] The effect of bead size was less evident. For example, between T100-20 and T25-20, there was no difference in strain at maximum stress; for T100-50/T25-50 and U100-20/U25-20, larger bead size suggested lower strain capability. Comparison between U25-50 and U100-50, showed that U25-50 behaved more brittlely than expected. Overall strain capability of the composite was reduced by surface treatment of the beads.

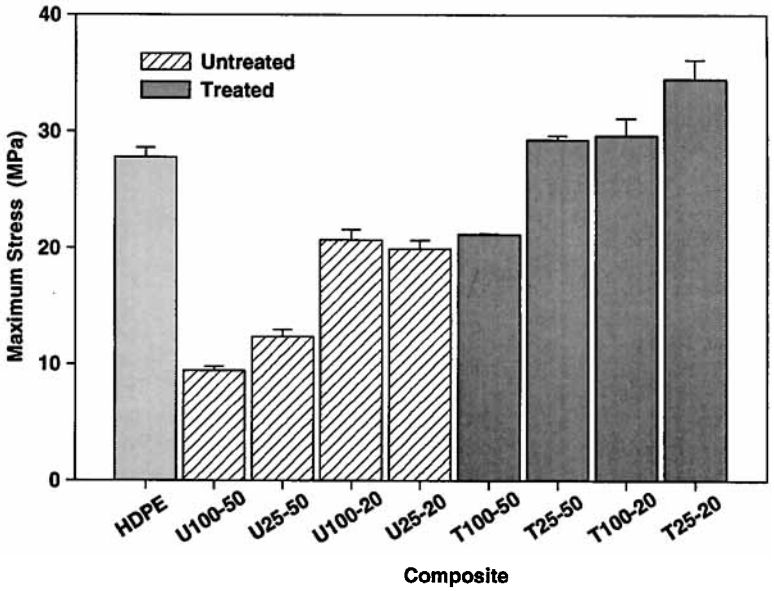

Figure 5 Maximum stress results from tensile testing grouped according to treatment. Tests done at 10 mm/min, 20°C.

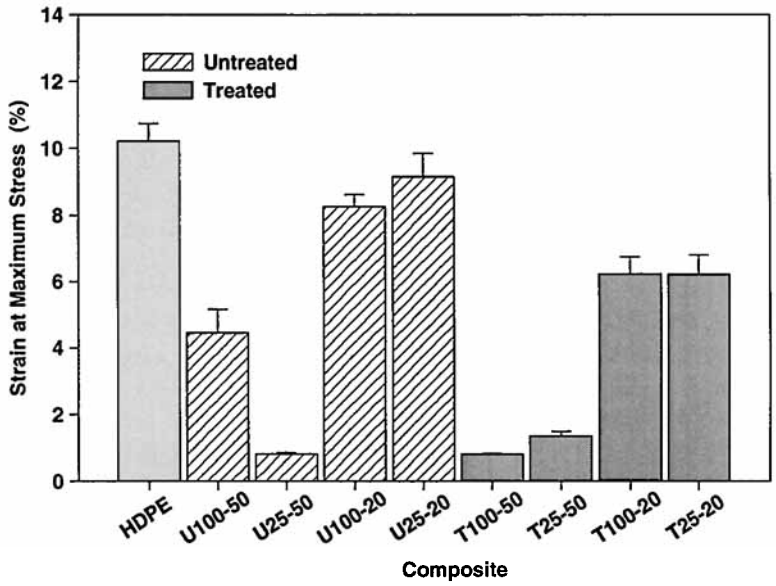

Figure 6 Strain at maximum stress results from tensile testing grouped according to treatment. Tests done at 10 mm/min, 20°C.

Two modulus measurements are shown in Table VII. The secant modulus (E_s) was calculated by the Instron software using a point at 90% of the maximum load. This was considered to represent average elastic behavior. The initial modulus (E_i) was calculated using the Instron Series IX automodulus function. Secant moduli for composites with 50% filler were higher than those with 20% filler. The exception was U100-50, which had a modulus much lower than expected. Ignoring U100-50 and U25-50 for the moment, Figure 7 shows that the modulus is independent of bead size. This is in accordance with other data.[38,39] Comparison of results based on surface treatment shows that modulus increases with increasing adhesion.

The low modulus of U100-50 and the low strain capacity of U25-50 was puzzling. Examination of these samples with a scanning electron microscope

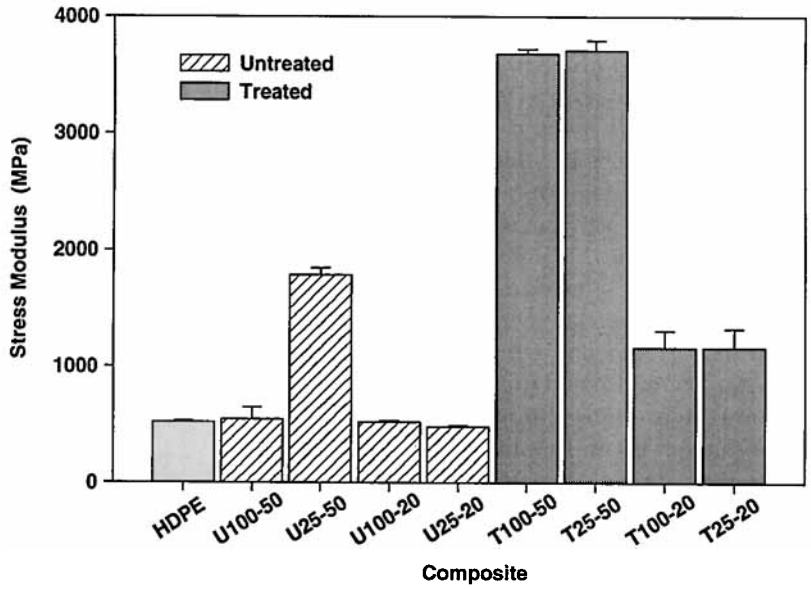

Figure 7 Secant modulus results from tensile testing grouped according to treatment. Tests done at 10 mm/min, 20°C.

showed that the calculated filler concentrations were reasonable and that there was good dispersion. The cause for the anomalous behavior remains unanswered.

The ratio of initial modulus to secant modulus (E_i/E_s) gave a measure of the degree of nonlinearity seen in a stress–strain curve before maximum stress. Higher ratios corresponded with larger nonlinearities. Ranking the composites from lowest to highest E_i/E_s gave: U25-50, T100-50, T25-50, T100-20, HDPE, T25-20, U100-50, U100-20, and U25-20. It can be seen that the treated composites behaved in a more linear manner than the untreated composites. Also, higher filler concentration and larger bead size tended to suppress nonlinear behavior.

Comparison of Experimental to Theoretical Results

The objective of comparing model predictions to experimental data is to evaluate the model's capability of accounting for changes in mechanical behavior due to changes in particle size, filler volume fraction and adhesion energy. Table VIII shows the parameters used for the model. Model parameters from composites T100-50 and T25-50 were chosen as baselines from which to compare other parameters. The anomalous behavior exhibited by U100-50 and U25-50 made using these composites as baselines less desirable.

The known parameters for composites T100-50 and T25-50 were: (1) the particle size and distribution, (2) the filler volume fraction, (3) the matrix mechanical properties, and (4) the filler mechanical properties. The unknown parameters for each of the composites were: (1) the maximum packing fraction and (2) the adhesion energy. These parameters had to be determined by trying different values in the model and then comparing the predicted behavior with the observed behavior. When the predicted results corresponded with the observed results, then the correct values for the unknown parameters had been found. The void content for these particular composites was assumed to be zero because it was not possible to determine it experimentally without knowledge of the actual filler volume fraction.

According to Eqs. (5) and (6), the maximum packing fraction, P_f, and the matrix shear modulus, G_m, have a direct influence on the final composite modulus. Using a measured secant modulus of 500 MPa and a Poisson ratio of 0.34,[40] a shear modulus of 187 MPa was calculated for G_m. Secant modulus was used instead of initial modulus in order to accommodate the linear elastic assumption made in the model. By trying a range of values between 0.4 and 1.0 for P_f, good agreement between predicted and measured modulus for both T100-50 and T25-50 was found using a value of 0.6. This value corresponds with the maximum packing fraction for loose random packed spheres.[41]

Equation (3) states that the strain and hence, the stress, is dependent on the adhesion energy. All the composites exhibited a maximum stress point so the adhesion energy was found by selecting a value that

Table VIII Model Input Parameters for Selected Composites

	T100-50 (Baseline)	T25-50 (Baseline)	T100-20	T25-20	U25-50	U25-20
Avg. rad.[a] (μm)	65	15.5	65	15.5	15.5	15.5
Log std. dev.[a]	0.0374	0.167	0.0374	0.167	0.167	0.167
V_f[a]	0.49	0.49	0.19	0.22	0.48	0.19
V_v	0.0	0.0	0.0	0.0	0.01	0.03
P_f[c]	0.6	0.6	0.6	0.6	0.6	0.6
G_f[b] (GPa)	30	30	30	30	30	30
G_m[a] (MPa)	187	187	187	187	—	—
G_m-fit[c] (MPa)	—	—	—	—	100	115
ν_f[b]	0.16	0.16	0.16	0.16	0.16	0.16
ν_m[b]	0.34	0.34	0.34	0.34	0.34	0.34
G_c[c] (N m/m^2)	9.7	7.2	—	—	—	—
G_c-fit[c] (N m/m^2)	—	—	35	14	2.5	8.5

[a] Measured value.
[b] Value quoted from literature.
[c] Value found by numerical trial and error. -fit, value required to obtain correspondence between observed and predicted behavior. V_f, filler volume fraction. V_v, void volume fraction. G_f, filler shear modulus. G_m, matrix shear modulus. ν_f, filler Poisson ratio. ν_m, matrix Poisson ratio. G_c, adhesion energy.

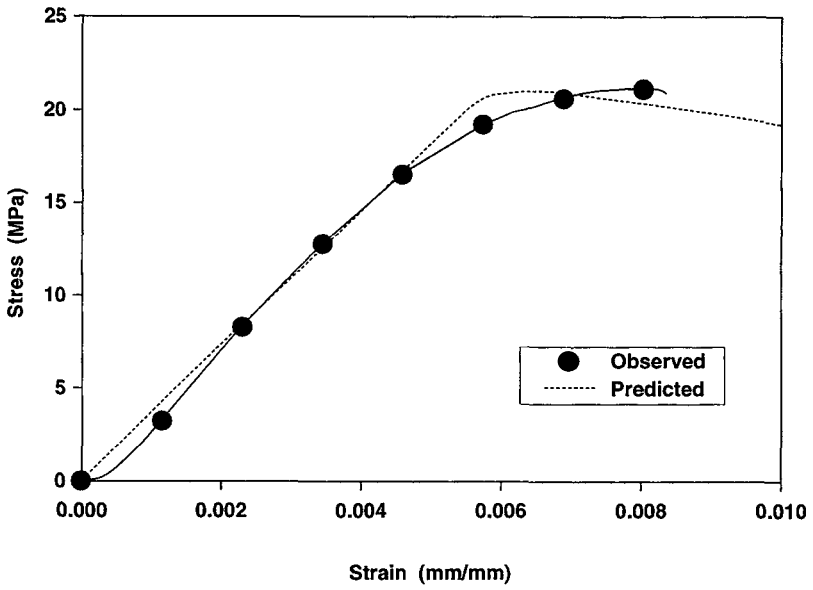

Figure 8 Comparison of predicted and observed tensile test results for T100-50. Tests done at 10 mm/min, 20°C.

would reproduce the observed maximum stress. This method was used by Anderson.[27] For T100-50, a value of 9.7 N m/m^2 gave the desired result while for T25-50, 7.2 N m/m^2 worked well. The different adhesion energies found may be due to variations in surface treatment between the two composites. Ideally, if surface treatment was the same, the adhesion energies would be the same. The adhesion energies could also reflect the difference in bead surface area available for bonding in the two composites. T25-50 has more total surface area than T100-50 so less adhesion energy would be required overall. Figures 8 and 9 show a comparison between the predicted and observed behaviour for T100-50 and T25-50.

The present results for T100-50 and T25-50 demonstrate that the model gives reasonable predictions for composite mechanical behavior when considering the effects of particle size, good adhesion, and high filler volume fraction. The model also

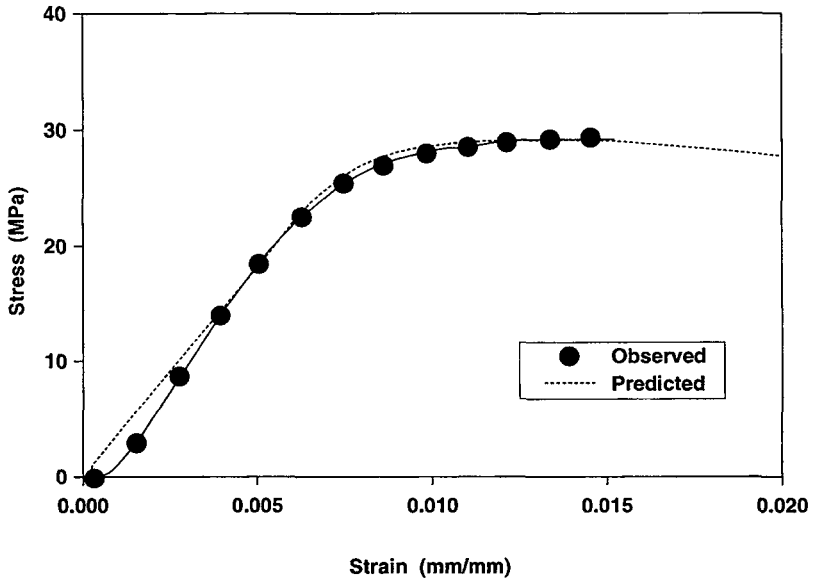

Figure 9 Comparison of predicted and observed tensile test results for T25-50.

produces a reasonable maximum packing fraction when it is back-calculated from measured properties.

Using the T100-50 maximum packing fraction, matrix shear modulus, and adhesion energy as input parameters for T100-20, a discrepancy between predicted behavior (curve marked "expected") and observed behavior is evident (Fig. 10). The figure shows that the maximum strength is underpredicted. Furthermore, when the predicted maximum stresses for T100-50 and T100-20 are compared, T100-50 is stronger than T100-20. However, comparison of the observed maximum stresses for T100-50 and T100-20 show that T100-50 is weaker than T100-20. The experimental result follows the trend seen in the literature.[41] For nonpolar polymers above their T_g, strengths begin to fall when the relative filler volume, V_f/P_f, is higher than 0.3.

The inability of the model to correctly predict the drop in strength may be attributed to assumption 3 (see Theory). It was stated that the composite could be considered homogeneous so that average stresses could be used. This assumption effectively excluded the possibility of having stress concentrations on a microscopic scale in the composite. In reality, the 50% composite contained many more stress concentrations than the 20% composite. Consequently, the average stress in the composite was raised and this made it weaker. The increased number of stress concentrations also increased the number of sites from which cracks could form.[42] In order to regain the observed maximum stress for T100-20 in the model, the adhesion energy had to be increased above the T100-50 value. The curve marked "fitted" in Figure 10 shows a comparison between the predicted behavior using the T100-20 "G_c-fit" parameter (Table VII) and the observed behavior.

The predicted behavior of T25-20 using the T25-50 modulus and adhesion energy parameters shows that the maximum strength is again too low (Fig. 11, "expected" and "observed" curves). Given this result, it is apparent that the prediction for T25-20 has the same problem as the prediction for T100-20. Employing the argument that stress concentrations were the cause of the discrepancy, the subsequent increase in the model adhesion energy can be resolved.

Evaluation of the mechanical behavior for a composite containing untreated filler initially proceeded by using the matrix modulus and 10% of the adhesion energy found for the equivalent composite containing treated beads. For example, U25-50 used a matrix shear modulus of 187 MPa and an adhesion energy of 0.72 N m/m^2. Void content was also included in the modulus calculations to see if it played a significant role in the results. Assuming the lower densities of the U series of composites were due to voids while the higher densities of the T series of composites were due to the absence of voids, void content was calculated using ASTM D2734.[43] Inspecting the expected and observed curves of U25-50 in Figure 12, it is evident that even with the inclusion of void content in the modulus calculations, the expected modulus remained higher than the observed modulus.

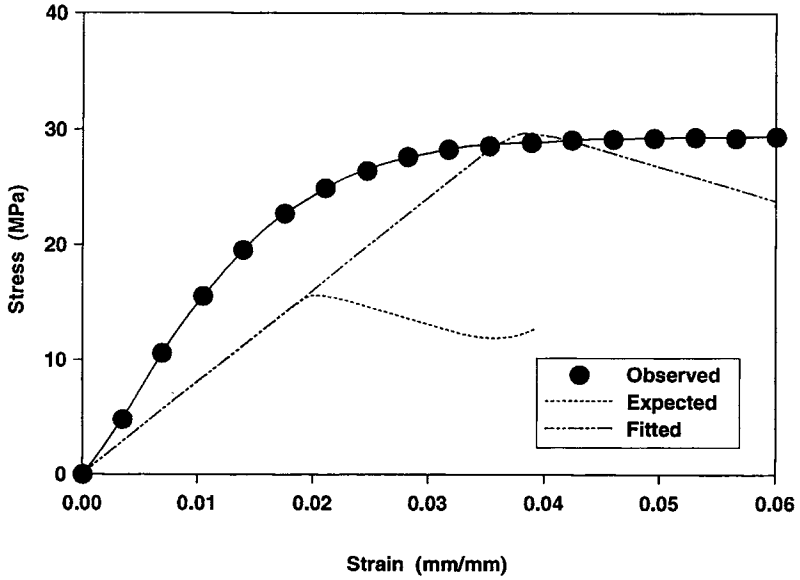

Figure 10 Comparison of expected, fitted, and observed tensile test results for T100-20.

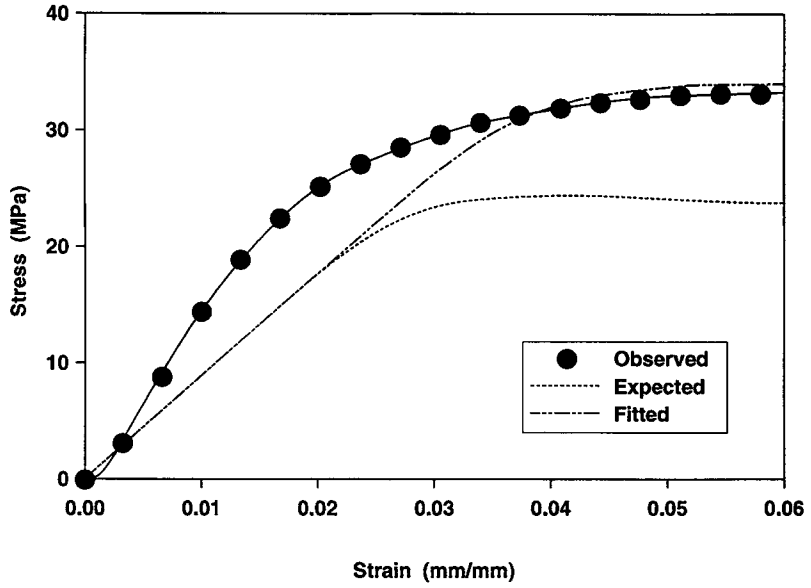

Figure 11 Comparison of expected, fitted, and observed tensile test results for T25-20.

The reason for this incongruity may be attributed to the model's inability to account for the effects of localized straining. In T25-50, the silane coupling agent promoted adhesion at the filler–matrix interface. When the composite was loaded, the low modulus matrix was forced by the good adhesion to become highly deformed since the high modulus filler could not deform very much. In U25-50, the poor bonding between filler and matrix resulted in early particle debonding and void formation. Consequently, a lower modulus was measured because of the loss in reinforcement and the lack of strain in the matrix. This also explains why higher strains are seen for the U-series composites while lower ones are seen for the T-series composites (Table VI).

The fact that the observed and predicted U25-50 maximum strengths differed was not surprising. After fitting the model to the observed maximum stress for U25-50, a reasonable correspondence between fitted and observed behavior may been seen (Fig.

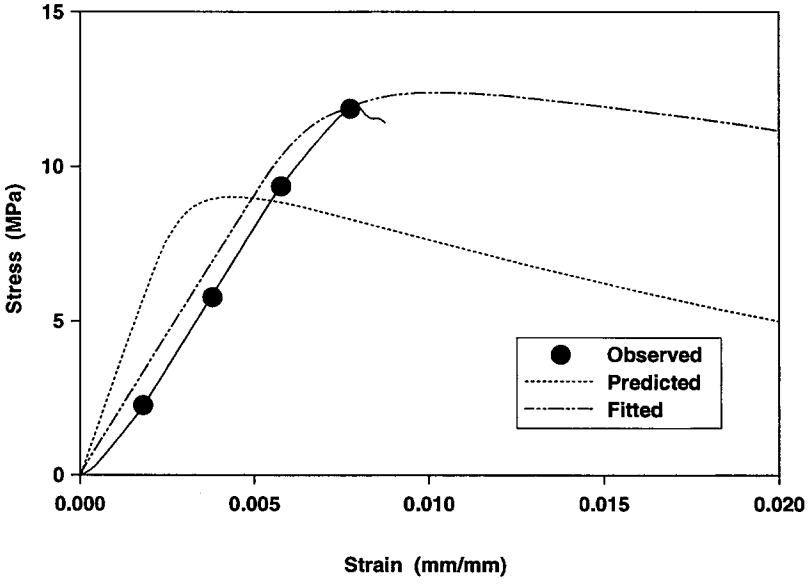

Figure 12 Comparison of expected, fitted, and observed tensile results for U25-50. Tests done at 10 mm/min, 20°C.

12). Table VII shows that the adhesion energy required to fit U25-20 data was higher than the adhesion energy required to fit U25-50 data. This occurred because the observed maximum stress of U25-20 was higher than the observed maximum stress of U25-50. Thus, the model's inability to account for stress concentrations affected the predictions for the U-series composites as well.

When the predicted and observed stress–strain curves are compared for T25-50 and U25-20, the effect of the model assumptions on the predictions becomes apparent. For composites such as T25-50, which have high solids loading and good adhesion, debonding has a greater influence on the overall nonlinearity. The probability of survival curve in Figure 13 shows that the particles theoretically start to debond near point *A*. Before point *A*, good agreement is seen between predicted and observed results because the increased adhesion required that much more load be applied to the composite before debonding took place. This promoted linear behavior.[38] After point *A*, the correspondence of the predicted stress decrease with the lower particle survival indicates most of the nonlinearity is due to loss of reinforcement. The correspondence between the theoretical and experimental results demonstrates that the model works well for this configuration.

For composites such as U25-20, which have low solids loading and poor adhesion, nonlinear matrix behavior has a greater influence. Examination of Figure 14 before point *B* reveals nonlinear behavior occurring in the test specimen before the particles theoretically start to debond. After point *B*, particle debonding accounts for the observed mechanical behavior quite well. Poorer correspondence between predicted and observed behavior shows that nonlinear matrix behavior should be taken into account particularly for lowly loaded composites. If the T25-50 nonlinearity was considered to be debond dominated and the U25-20 nonlinearity was considered to be matrix dominated, the E_i/E_s ratios in Table VII would suggest that nonlinearities in U25-50, T100-50, and T100-20 were debond dominated while the nonlinearities in T25-20, U100-50, and U100-20 were matrix dominated.

There are various mechanical and chemical methods to assess adhesion energy.[44–48] Measured values for adhesion energy range from 0.07 to 0.30 N m/m^2 between silica particles and ethylene vinyl acetate[49] to 5 N m/m^2 for glass beads and polyurethane.[27] Given the magnitude of the energies found using the model, it is unlikely that they are realistic because the effects of stress concentration and localized straining were neglected. Furthermore, the reduction of the debonding problem to a simple separation of matrix and filler precluded the possibility of partial debonding.[50] Therefore, adhesion energy can be considered, in this case, to be a parameter that groups together the effects of adhesion and other interfacial phenomena. Although the model oversimplifies the debonding process, it does provide a convenient mechanism for relating the composite

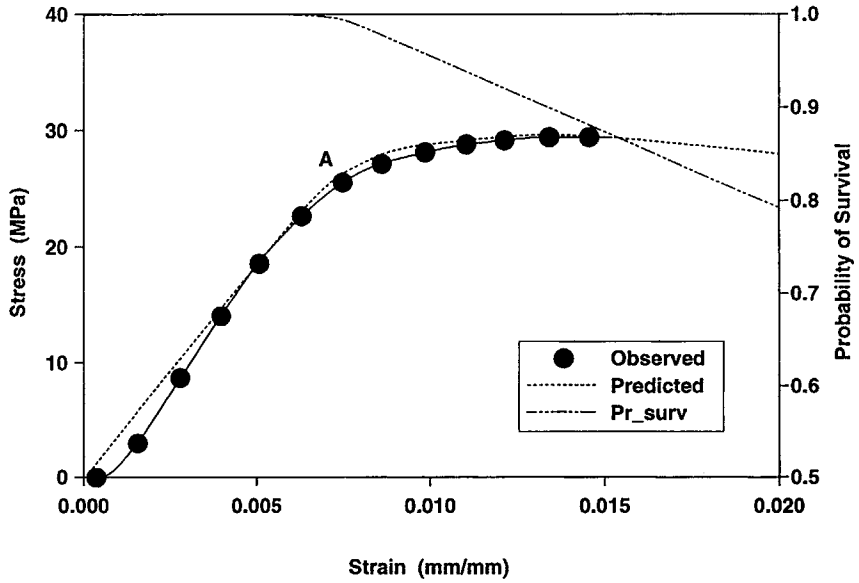

Figure 13 Illustration of nonlinearity due to particle debonding in T25-50.

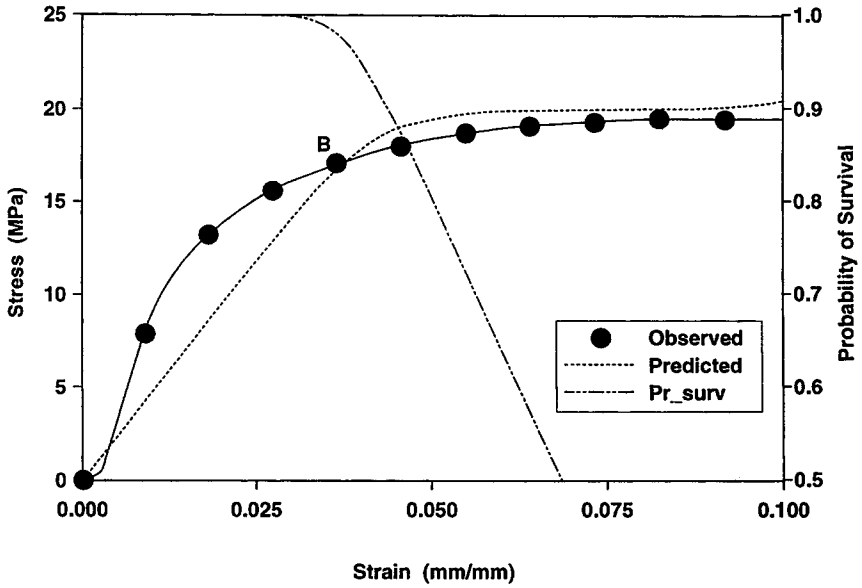

Figure 14 Illustration of nonlinearity due to matrix behavior in U25-20.

modulus and stress–strain state to the loss of reinforcement without requiring a micromechanical description that is too cumbersome to manage.

CONCLUSIONS

A comparison between observed and predicted results showed that the Anderson–Farris model could predict the mechanical behavior of highly loaded composites if a representative value for adhesion energy was available. Good results for these composites were obtained because, overall, they behaved in a linear manner and they had significant numbers of particles to debond. Comparison of results for lowly loaded composites pointed out the model's need to take into account stress concentrations. Predictions suggested that maximum stress would always increase with filler concentration. However, experimental data showed that it decreased at the higher filler concentrations. Examination of results for composites containing treated and untreated beads demonstrated the influence that localized straining had on mechanical behavior. The inability of the model to reproduce the observed results showed that this was another deficiency that needed to be addressed. Although the model has its shortcomings, the use of adhesion energy to relate loss of reinforcement to changes in modulus provides a convenient starting point for further work.

The authors would like to thank the Defence Research Establishment Valcartier (DREV) management for their support of this work. Special thanks goes to Mr. Gerald Duquet and staff at the DREV Plastics Shop for their help in fabricating the test specimens and to the departmental machine shop staff at Laval University for their help in fabricating the HDPE and glass bead screw feeders. The authors would also like to thank Mr. Brahim Brahimi for his assistance in the setup and repair of the Haake Buchler equipment. The generosity of Dow Chemical Canada Inc., Potters Industries Ltd., and Union Carbide Chemicals and Plastics Canada Inc. are also acknowledged.

REFERENCES

1. H. S. Katz and J. V. Milewski, Eds., *Handbook of Fillers for Plastics,* Van Nostrand Reinhold, New York, 1987, p. 3.
2. G. Lubin, Ed., *Handbook of Composites,* Van Nostrand Reinhold, New York, 1982, p. 1.
3. J. Leidner and R. T. Woodhams, *J. Appl. Polym. Sci.,* **18,** 1639 (1974).
4. M. Morton, R. J. Murphy, and T. C. Cheng, *Adv. Chem. Ser.,* **142,** 409 (1974).
5. G. Landon, G. Lewis, and G. F. Boden, *J. Mater. Sci.,* **12,** 1605 (1977).
6. D. W. Nicholson, *J. Adhesion,* **10,** 255 (1979).
7. J. C. Smith, G. A. Kermish, and C. A. Fenstermaker, *J. Adhesion,* **4,** 109 (1972).
8. P. Dreyfuss, A. N. Gent, and J. R. Williams, *J. Polym. Sci.: Polym. Phys. Ed.,* **18,** 2135 (1980).
9. B. Pukanszky, *Composites,* **21,** 255 (1990).

10. J. A. King, D. A. Buttry, and D. F. Adams, *Polym. Comp.*, **14,** 292 (1993).
11. F. R. Schwarzl, Central Laboratory TNO Delft (Netherlands), CL-64/49, 1964.
12. M. Sumita, T. Ookuma, K. Miyasaka, and K. Ishikawa, *J. Appl. Polym. Sci.*, **27,** 3059 (1982).
13. S. N. Maiti and P. K. Mahapatro, *J. Appl. Polym. Sci.*, **42,** 3101 (1991).
14. R. L. Hewitt and M. C. deMalherbe, *J. Comp. Mat.*, **4,** 280 (1970).
15. J. C. Halpin and J. L. Kardos, *Polym. Eng. Sci.*, **16,** 344 (1976).
16. R. F. Fedors, *Polymer*, **20,** 324 (1979).
17. Z. Hashin and S. Shtrikman, *J. Mech. Phys. Solids*, **11,** 127 (1963).
18. L. J. Walpole, *J. Mech. Phys. Solids*, **14,** 151 (1966).
19. J. Korringa, *J. Math. Phys.*, **14,** 509 (1973).
20. Z. Hashin, *J. Mech. Phys. Solids*, **40,** 767 (1992).
21. Z. Hashin, *J. Appl. Mech.*, **50,** 481 (1983).
22. N. Laws and R. McLaughlin, *J. Mech. Phys. Solids*, **27,** 1 (1979).
23. F. Lene and D. Leguillon, *Int. J. Solids Struct.*, **18,** 443 (1982).
24. R. A. Schapery, *Eng. Frac. Mech.*, **25,** 845 (1986).
25. Y. P. Qiu and G. J. Weng, *J. Appl. Mech.*, **59,** 261 (1992).
26. L. L. Anderson and R. J. Farris, *Polym. Eng. Sci.*, **28,** 522 (1988).
27. L. L. Anderson, Ph.D. Dissertation, U. of Massachusetts, 1989.
28. T. R. Tauchert, *Energy Principles in Structural Mechanics*, McGraw-Hill, New York, 1974, p. 43.
29. J. N. Farber and R. J. Farris, *J. Appl. Polym. Sci.*, **34,** 2093 (1987).
30. Organofunctional Silanes, Union Carbide Chemicals product literature, 1991.
31. *Solid Propellant Mechanical Behaviour Manual*, Chemical Propulsion Information Agency, Publ. 21, 1970, p. 4.3.2-1.
32. Density and Specific Gravity (Relative Density) of Plastics by Displacement, ASTM D792-86, 1987.
33. M. Takayanagi, *Pure Appl. Chem.*, **15,** 555 (1967).
34. D. M. Hoffman and B. M. McKinley, *SPE ANTEC*, 261 (1984).
35. R. B. Seymour, *Polymers for Engineering Applications*, ASM International, 1987, p. 57.
36. D. Saylak, *Appl. Polym. Symp.*, **1,** 247 (1965).
37. L. E. Nielsen, *Mechanical Properties of Polymers and Composites*, Vol. 2, Marcel Dekker, New York, 1974, p. 405.
38. U. Yilmazer and R. J. Farris, *J. Appl. Polym. Sci.*, **28,** 3369 (1983).
39. A. E. Oberth, *Rubber Chem. Tech.*, **40,** 1337 (1967).
40. J. A. Sauer and K. D. Pae, in *Introduction to Polymer Science and Technology: An SPE Textbook*, H. S. Kaufman and J. J. Falcetta, Eds., Wiley, New York, 1977, p. 392.
41. T. H. Ferrigno, in *Handbook of Fillers for Plastics*, H. S. Katz and J. V. Milewski, Eds., Van Nostrand Reinhold, New York, 1987, pp. 35–38.
42. L. R. Cornwall and R. A. Schapery, *Metallography*, **8,** 445 (1975).
43. Void Content of Reinforced Plastics, ASTM D2734-70, 1988.
44. A. N. Gent and G. L. Liu, *J. Mater. Sci.*, **31,** 2467 (1991).
45. P. J. Herrera-Franco and L. T. Drzal, *Composites*, **23,** 2 (1992).
46. W. C. Hamilton, *J. Colloid Interface Sci.*, **47,** 672 (1974).
47. D. K. Owens and R. C. Wendt, *J. Appl. Polym. Sci.*, **13,** 1741 (1969).
48. F. M. Fowkes, D. O. Tischler, J. A. Wolfe, and M. J. Halliwell, *Org. Coating Appl. Polym. Sci. Proc.*, **46,** 1 (1982).
49. S-W. Shang, Ph.D. Dissertation, U. of Florida, 1989, p. 141.
50. Y. Sato and J. Furukawa, *Rubber Chem. Tech.*, **35,** 857 (1962).

Received December 17, 1993
Accepted January 29, 1994